Available online at www.sciencedirect.com
SCIENCE DIRECT
International Journal of Mass Spectrometry 249–250 (2006) 31–44
International Journal of Mass Spectrometry
www.elsevier.com/locate/ijms

State-selected $C_2H_2^+ + C_2H_4$ reaction: Controlled by dynamics or statistics?

Hartmut Palm, Christian Alcaraz, Philippe Millié, Odile Dutuit *

Laboratoire de Chimie Physique, UMR8000, CNRS-UPS, Bât. 350, Centre Universitaire Paris-Sud, France

Received 30 December 2005; received in revised form 4 January 2006; accepted 5 January 2006
Available online 3 February 2006

This paper is dedicated to Chava Lifshitz, who was a great scientist with deep human qualities. She remains an example for women scientists.

Abstract

The reaction between acetylene ion and ethylene is revisited to investigate possible dynamical effects in one of the reactions, which are considered as benchmark systems for statistical models. Reactant ions are produced by photoionisation with synchrotron radiation and are selected in internal energy by a coincidence method between threshold photoelectrons and photoions. Measured absolute reaction cross-sections decrease with collision energy (0.1–1 eV CM), but increase with acetylene ion vibrational energy for the three exothermic channels giving $C_4H_5^+$, $C_3H_3^+$ and $C_2H_4^+$ ionic products. Even though RRKM calculations are shown to fit rather well experimental results for both the bimolecular ($C_2H_2^+ + C_2H_4$) and unimolecular ($C_4H_6^+$) systems, some experimental results clearly indicate dynamical effects in this reaction for the $C_2H_4^+$ production channel, in particular the strongly backward peaked $C_2H_4^+$ angular distribution. We propose an alternative model combining reaction control both by dynamics and by statistics: the first step in the reactant approach is the capture between reactants, followed by a charge transfer process controlled by dynamics. In a second step, either the two reactants separate leading to $C_2H_4^+$ ionic products, or there is a rearrangement into 1,3-butadiene ($C_4H_6^+$) ion which dissociates statistically into $C_4H_5^+ + H$ and $C_3H_3^+ + CH_3$ products. Charge transfer is shown to be possible at intermediate intermolecular distances, slightly shorter than the capture distance, provided that one takes into account the charge–quadrupole interaction in addition to the ion-induced dipole interaction. This work clearly shows that a good fit of experimental data by RRKM calculations does not prove that the reaction elementary mechanism is controlled by statistics.

Keywords: Ion–molecule reaction; Photoionisation; Coincidence; Dynamic; Statistical theory

1. Introduction

The simple picture of reaction elementary mechanisms being controlled by dynamics for small systems (three to four atoms) and by statistics for systems involving more than four atoms [1,2] has been recently more and more questioned by several authors [3–5] (and references therein). In this paper, the $C_2H_2^+ + C_2H_4$ reaction is revisited to investigate possible dynamical effects in a reaction which is considered as a benchmark system for statistical models [6]. Two questions will be addressed: (i) when is it justified to use statistical theories to describe a reaction mechanism? (ii) Is a good fit of experimental data by statistical models a proof that the reaction is controlled by statistics? The aim of this work is to present a set of experimental data for the $C_2H_2^+ + C_2H_4$ reaction [7], as complete as possible, to give the maximum number of constraints to the application of statistical theories. It involves in particular the effect of internal energy excitation of $C_2H_2^+$ reactant ions on the reactivity.

From an experimental point of view, reaction mechanisms have been divided into two categories: direct or impulsive collisions and complex-mediated reactions. The rotation period of the collision intermediate serves as an internal "kinematic clock", which can be used to distinguish between the two types of mechanisms [8]. They manifest themselves by the product ion angular distributions which are asymmetric or symmetric with respect to the centre of mass for "direct" or "intermediate complex" mechanisms, respectively. The lifetime of these complexes ranges from 10^{-13} to 10^{-6} s and if it is much longer than a rotational period ($\tau = 10^{-12}$ to 10^{-13} s), they are referred to as "long-lived complexes" [8]. In polyatomic systems, when the collision energy

* Corresponding author. Tel.: +33 1 69 15 56 18; fax: +33 1 69 15 30 53.
E-mail address: odile.dutuit@lcp.u-psud.fr (O. Dutuit).

1387-3806/$ – see front matter © 2006 Published by Elsevier B.V.
doi:10.1016/j.ijms.2006.01.005

does not exceed about 1 eV, long-lived complex mechanisms are usually supposed to dominate the reaction dynamics.

As the number of degrees of freedom is very often too big to perform a complete quantum theory treatment, statistical model approaches originally developed for unimolecular fragmentation (see for example the review paper of Lifshitz [9]), are applied to the intermediate complex. Thus, statistical theories such as the theory developed by Rice, Ramsperger, Kassel and Marcus (RRKM) or the phase space theory (PST), are applied to calculate the reaction cross-section and the product ion branching ratio resulting from the dissociation of the complex [1]. These theories implicitly suppose a statistical randomisation of the total energy into all vibrational modes of the intermediate complex, prior to its dissociation. However, this randomisation by intramolecular vibrational redistribution (IVR) can occur on a time scale similar or much longer than the dissociation time [10]. Moreover, if the initial state is electronically excited, it often also implicitly involves a rapid internal conversion towards the ground state prior to vibrational energy redistribution in the ground state, which is not necessarily the case [11]. Therefore the binary assessment of "direct" reactions controlled by dynamics and "complex-mediated" reactions controlled by statistics on the ground potential energy surface is obviously too simple.

Our group has studied the reaction of acetylene ions with small hydrocarbon molecules (methane, ethylene and ethane) to explore the applicability of the above-mentioned concepts to medium-size (about 10 atoms) polyatomic systems. Their reaction channels are very diverse, such as charge transfer, hydrogen atom (H, H^+ and H^-) transfers and reactions involving the exchange of the heavier C-atoms. In such ion–molecule reactions, in particular the $C_2H_2^+ + C_2H_4$ reaction, one expects in a first step the formation at long intermolecular distance of a non-covalent polarisation complex $(C_2H_2–C_2H_4)^+$ in the collision approach between the reactants. The system can then rearrange towards the deep well, corresponding to the most stable covalent molecular ionic structure of the intermediate complex $C_4H_6^+$, which is the butadiene ion. In this case, as well as for the $C_4H_8^+$ system, Chesnavich et al. [12] have developed a statistical model with two transition states at long and short intermolecular distances, called the "transition state switching statistical model". This model is used and discussed in the present study, by fitting the experimental product ion branching ratios with the parameters of the transition state between the polarisation complex and the long-lived butadiene intermediate complex.

Let us note that starting with the $C_2H_2^+ + C_2H_4$ reaction means entering into the $C_4H_6^+$ system on an excited potential energy surface, the ground potential energy surface corresponding to the $C_2H_4^+ + C_2H_2$ dissociation limit. This implies either a dynamical reaction jump from one surface to the other or an internal energy conversion process at shorter intermolecular distances. Nevertheless, quite accurate information on the relevant potential minima and transition states of the ground state surface have been obtained [13]. On the contrary, very sparse data are known for the first excited state of the $C_4H_6^+$ system (which is adiabatically connected to the $C_2H_2^+ + C_2H_4$ entrance channel).

Dynamical effects are expected in particular when reactant ions are vibrationally excited, due to a bad coupling between the high frequency vibrational modes of the reactant ion and the low frequency intermolecular vibrational modes of the polarisation complex. The resulting intramolecular vibrational redistribution (IVR) is then slow and the randomisation can be only partial [14]. State-selected experiments are particularly suited to show the limitation of statistical theories [15–17]. Hence non-statistical effects have been observed for several reactions, such as the H_2CO^+ and $C_2H_2^+$ reactions with methane [5], where the reactivity strongly depends on the excited vibrational mode of the reactant ion.

The reaction of acetylene ions $C_2H_2^+$ with neutral ethylene molecules C_2H_4 has been investigated in the gas phase with different experimental techniques (see for example [18,19,6]) over the last three decades. The dissociation of the intermediate species of this reaction, $C_4H_6^+$, has also been studied by ionisation of different C_4H_6 isomers by photons or electron impact [20–27]. The combined study of the bimolecular ion–molecule reaction and the unimolecular ion dissociation allows to check if the system explores or not the deepest butadiene ion potential energy well.

Only the following exothermic channels of the $C_2H_2^+ + C_2H_4$ reaction are considered in this work, which are the only reaction channels observed in the energy range investigated in the present study (about 1 eV for both the internal and the collision energy):

$$C_2H_2^+ + C_2H_4 \rightarrow C_4H_5^+ + H, \quad \Delta H = -1.76\,\text{eV} \qquad (1)$$

$$C_2H_2^+ + C_2H_4 \rightarrow C_3H_3^+ + CH_3, \quad \Delta H = -1.69\,\text{eV} \qquad (2)$$

$$C_2H_2^+ + C_2H_4 \rightarrow C_2H_4^+ + C_2H_2, \quad \Delta H = -0.89\,\text{eV} \qquad (3)$$

where ΔH is the exothermicity for each reaction channel, calculated with the heat of formations derived from Lias et al. [28]. Channels (1) and (2) involve heavy atom transfer and most probably result from a long-lived intermediate complex mechanism. Channel (3) corresponds to a charge transfer between the reactants. There is another possible exothermic channel, i.e.,

$$C_2H_2^+ + C_2H_4 \rightarrow C_4H_4^+ + H_2, \quad \Delta H = -1.77\,\text{eV} \qquad (4)$$

which is measured as a very minor channel in this work, even though it is the most exothermic channel. A study of the butadiene ion dissociation [21,23] also shows that this fragment ion is minor with an appearance energy of about 2.5 eV above the butadiene ionisation potential, corresponding to a substantial shift versus the thermochemical energy onset. This channel will not been considered further in the present study.

2. Experimental

The experimental set-up, called CERISES (acronym for 'Collisions Et Réactions d'Ions Sélectionnés par Electrons de Seuil') has already been described in detail [29]. Reactant ions are produced by photoionisation with synchrotron radiation in the VUV range (11.4–12.5 eV). They are selected in internal energy using the Threshold PhotoElectron PhotoIon COincidence (TPEPICO) technique [30]. Reactions are studied using the guided ion beam technique [31,32] at controllable collision

energies ranging from 0.05 to about 1 eV in the centre of mass frame.

Briefly, the apparatus is divided into three differentially pumped sections, corresponding to source, reaction, and detection regions. Reactant ions are produced by photoionisation with synchrotron radiation from a bending magnet beam line of the Orsay Super-ACO storage ring. Monochromatized light is focused in the centre of the extraction region, which is filled with acetylene at a pressure of about 10^{-4} Torr. A modest dc-field (1.25 V/cm) extracts electrons and ions in opposite directions. Threshold electrons are selected by a combination of angular and time-of-flight discrimination. In the present work their resolution is about 30 meV. Internal energy selected reactant ions can be produced in two ways: (i) The photon energy is set to the ionization energy of the acetylene molecule, to obtain only acetylene ions in the vibrational ground state, (ii) state-selected vibrationally excited acetylene ions are produced by threshold photoelectron–photoion coincidences (TPEPICO). In the latter case, false coincidences are minimized by using temporally gated electrodes and a sweeping pulse method, and subtracted from the coincidence measurements by recording false coincidence spectra in the same experimental conditions [33].

Reactant ions formed in the source are injected into a first radiofrequency octopole ion guide which contains at its end a 4.4 cm long scattering cell, filled with the ethylene target gas. Pressures were maintained at about 10^{-4} Torr to ensure single collision conditions. A Baratron gauge is used to measure absolute pressures. Kinetic energies were varied between 0 and 3 eV in the laboratory frame (corresponding to the centre of mass energy E_{CM} = 0–1.56 eV) with a typical energy spread of about 120 meV (ΔE_{CM} = 62 meV). Product ions are extracted from the scattering cell into a second octopole, mass analyzed by a quadrupole mass filter and accelerated onto a multi-channel plate detector. Absolute reaction cross-sections with about 20% accuracy are obtained by this method. After careful calibration of the potentials applied along the ion trajectory, product ion time-of-flight spectra can be transformed to obtain projections of the velocity distributions on the time-of-flight axis [32,7]. Some of these time-of-flight spectra were obtained with a similar guided ion beam apparatus in Chemnitz, where acetylene ions were produced in their ground state by electron impact and collision relaxation in a high pressure storage source [7,34].

Acetylene from Air-Liquide is purified by passage through a dry ice trap. Deuterated compounds are used without further purification (purity > 95.5% per D-atom).

3. Results

3.1. Absolute cross-sections for the $C_2H_2^+ + C_2H_4$ reaction

Two kinds of absolute reaction cross-section measurements are made: reaction cross-sections of ground state $C_2H_2^+$ reactant ions as a function of collision energy and reaction cross-sections as a function of $C_2H_2^+$ internal energy at several fixed collision energies. In the first case, ground state $C_2H_2^+$ reactant ions are produced by photoionisation at 11.4 eV, which is the (0–0) ionization potential of acetylene. Parent and product ions are then

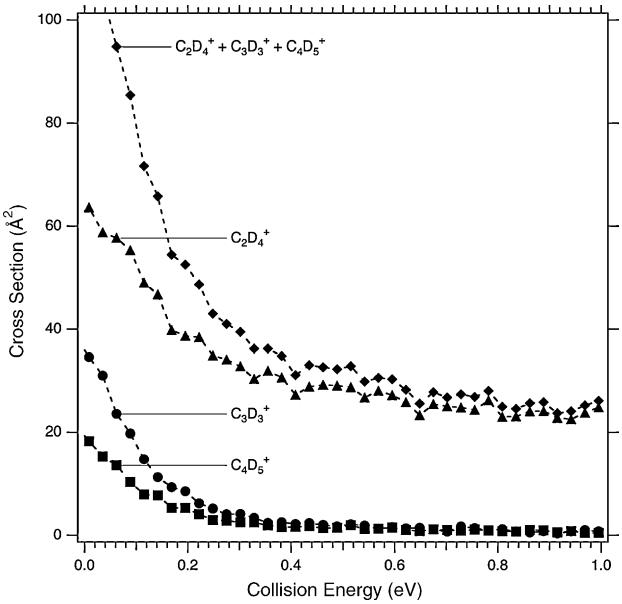

Fig. 1. Absolute cross-sections as a function of collision energy for the production of $C_2D_4^+$ (triangles), $C_3D_3^+$ (circles), $C_4D_5^+$ (squares) and the sum of the three (diamonds) in the $C_2D_2^+(X, v = 0) + C_2D_4$ reaction.

measured continuously and reaction cross-sections are obtained by using the general formula, which is approximated when the attenuation of the parent ion beam is lower than 10%:

$$\sigma = 1/nl_{cell} \times I/I_0$$

where l_{cell} is the effective reaction cell length, n the target gas density and I and I_0 are the number of parent and product ion counts normalized to the photon flux, respectively. The effective reaction cell length is calibrated with the cross-section of the $Ar^+ + D_2$ reaction giving $ArD^+ + D$ [35]. Deuterated acetylene and ethylene have been used to facilitate mass separation. No significant isotopic effect is expected for the kind of results obtained in the present study. This is corroborated by the study of the $C_2H_2^+ + C_2D_4$ and $C_2D_2^+ + C_2H_4$ reactions by Jarrold et al. [6], which gave the same results within experimental errors. Only absolute values of reaction cross-sections could slightly depend on the isotope, but this uncertainty is expected to be less than the experimental error. Fig. 1 shows the measured total absolute reaction cross-section as a function of collision energy, as well as partial absolute cross-sections for each reaction channel corresponding to the formation of $C_2D_4^+$, $C_3D_3^+$ and $C_4D_5^+$ product ions, respectively. The charge transfer channel giving $C_2D_4^+$ dominates at all collision energies and accounts for more than 90% of the product ion yield at collision energies above 0.5 eV.

Absolute reaction cross-sections have also been measured as a function of internal energy at several fixed collision energies. TPEPICO coincidence ion spectra have been recorded at the four photon energies corresponding, respectively, to the v = 0–3 vibrational states of the acetylene ion C–C ν_1 symmetric stretching mode. The threshold photoelectron spectrum of acetylene recorded in the photon energy region of the electronic ground state shows four main peaks, which correspond to this vibrational progression [36]. Absolute reaction cross-sections derived

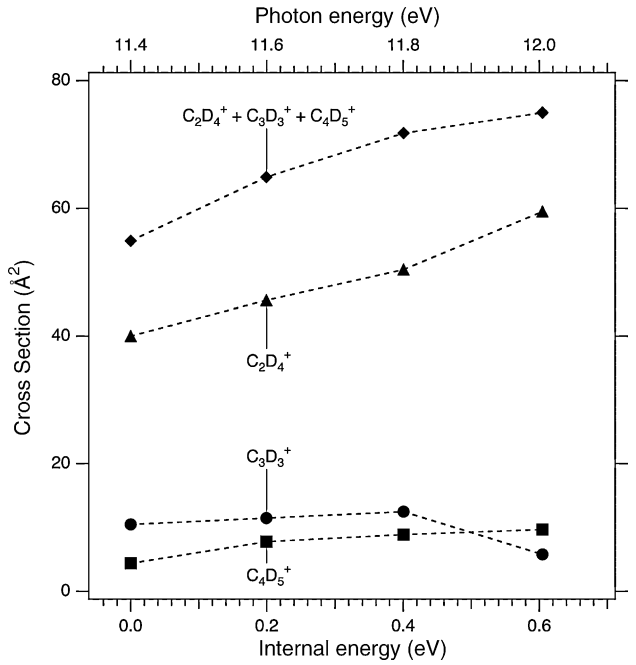

Fig. 2. Absolute cross-sections as a function of $C_2D_2^+$ internal energy for the production of $C_2D_4^+$ (triangles), $C_3D_3^+$ (circles), $C_4D_5^+$ (squares) and the sum of the three (diamonds) in the $C_2D_2^+(X, v) + C_2D_4$ reaction at a mean collision energy of 0.055 eV.

from these coincidence measurements are shown in Fig. 2 for $E_{CM} = 0.055$ eV. The total reaction cross-section value for the acetylene ions in the $v = 0$ ground state at this energy should be the same with both measurement methods (continuous mode and coincidence mode). Coincidence mode measurements systematically give lower values (see Figs. 1 and 2). The statistical error is higher for coincidence measurements, due to a much lower signal, but this does not entirely explain the discrepancy. A plausible explanation could be that only product ions arriving in a 1 ms time gate are recorded in the coincidence mode, very slow product ions might not be detected in this mode, leading to lower signals for products. However, relative values for the total and partial reaction cross-sections of ground state acetylene ions as a function of collision energy are in excellent agreement (not shown here). Both total and partial reaction cross-sections for each of the three channels increase with increasing vibrational energy of acetylene ions. To our knowledge, an increase of the reaction cross-section with internal energy of the reactants has never been observed for exothermic channels with polyatomic systems. This is only the case for small systems with three or four atoms, which are totally governed by dynamics [37–39]. Therefore the present result is very surprising. The cross-section value for $C_3D_3^+$ product ions for the $C_2D_2^+$ $v = 3$ state is probably too low, due to experimental uncertainties. It gives an estimate of the error bars on the absolute values of reaction cross-sections measured by this method, which are very difficult to estimate otherwise. For each vibrational state of $C_2D_2^+$, coincidence spectra have been recorded at several collision energies. All absolute reaction cross-sections obtained from those measurements (not shown in Fig. 2) show a decrease with collision energy, as for the ground state reactant ions. So the general trend of the cross-section, increasing with internal energy and decreasing with collision energy, is clearly established.

3.2. Product branching ratios for the unimolecular and bimolecular systems

The breakdown diagram for the dissociative photoionisation of C_4H_6 1,3-butadiene has been measured by Bombach et al. [23], using photoelectron–photoion coincidences. We have complemented this diagram with a higher internal energy of state-selected parent ion (see Fig. 3). This measurement has been done by photoionisation with synchrotron radiation of 1,3-butadiene at a photon energy of 13.5 eV and threshold photoelectron–photoion coincidences (TPEPICO). For this, we used another experimental set-up called SAPHIRS, which is a double electron and ion time-of-flight spectrometer, which has already been described in detail elsewhere [40]. The 13.5 eV photon energy corresponds to the asymptotic energy of the $C_2H_2^+ + C_2H_4$ reaction entrance channel. Our results are in good agreement with what could have been extrapolated at this energy from the diagram measured by Bombach et al. [23]. Solid lines are the result of a RRKM fit which will be presented below.

Product branching ratios for the unimolecular and bimolecular systems are compared in Table 1 at about the same total energy of the system, which is the asymptotic energy of the $C_2H_2^+ + C_2H_4$ reaction entrance channel. For the bimolecular system, it corresponds to reactant ions in their ground state and a collision energy of 0.055 eV. The branching ratio taken from the literature [6] has been measured for the reaction of ground state acetylene ions at 300 K, which corresponds to a mean value of the collision energy of about 0.06 eV. For the unimolecular system, this energy corresponds to a butadiene ion internal energy of

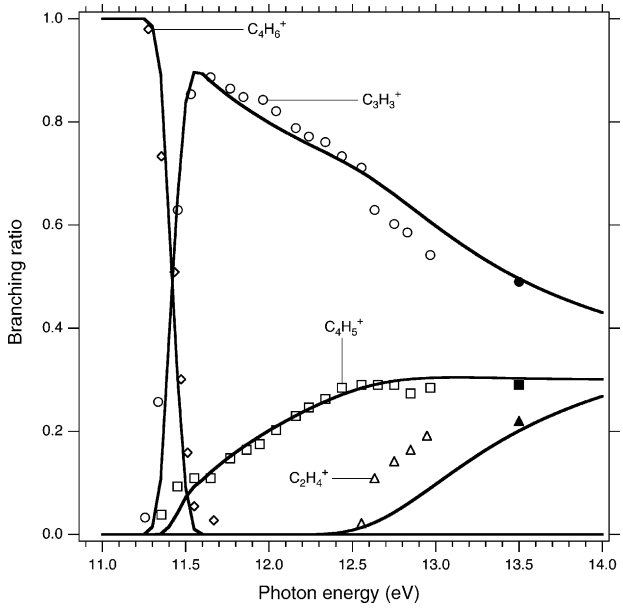

Fig. 3. Branching ratio in the dissociative photoionisation of 1,3-butadiene as a function of photon energy between parent ions $C_4H_6^+$ (diamonds) and fragment ions $C_2H_4^+$ (triangles), $C_3H_3^+$ (circles), and $C_4H_5^+$ (squares): experimental values from [23] (open symbols) and from this work (full symbols) and RRKM calculations (full lines) (see text for details).

Table 1
Product ion branching ratios for bimolecular and unimolecular reactions

	Branching ratio (%)		
	$C_2X_4^+$	$C_3X_3^+$	$C_4X_5^+$
Bimolecular reaction[a] (this work)	61	25	14
Bimolecular reaction[b] (Refs. [6,7])	64	20	16
Unimolecular reaction[c] (this work)	22	49	29

[a] For the $C_2D_2^+ + C_2D_4$ reaction at $E_{cm} = 0.062$ eV.
[b] For the $C_2H_2^+ + C_2H_4$ reaction at 300 K ($E_{cm} = 0.06$ eV).
[c] For the 1,3-butadiene ion with 4.44 eV internal energy, close to the $C_2H_2^+ + C_2H_4$ asymptotic energy.

4.44 eV (13.5–9.06 eV). Even though some measurements have been performed for deuterated species, which does not exclude a small isotope effect, the difference between the bimolecular and unimolecular product branching ratio is obvious: the bimolecular reaction strongly favours the $C_2H_4^+$ product ion, which is the minor product for the butadiene ion dissociation.

3.3. D/H scrambling in the $C_2H_2^+ + C_2H_4$ reaction

Hydrogen atom scrambling in the $C_2H_2^+ + C_2D_4$ reaction is checked by using normal acetylene and deuterated ethylene. Isotopomer branching ratios for each product ion are plotted as histograms in Fig. 4 for two different collision energies and ground state acetylene ion reaction. The third histogram displayed for each product ion results from a simple combinatorial calculation, assuming a complete statistical distribution of hydrogen atoms. Whereas $C_3X_3^+$ and $C_4X_5^+$ isotopomer product ions are very close to completely statistically scrambled, there is almost no scrambling in the $C_2X_4^+$ product ion formation. These results are in very good agreement with isotopic scrambling results measured by Jarrold et al. [6] at 300 K. The dominant $C_2X_4^+$ product ion is $C_2D_4^+$, corresponding to a simple charge transfer between $C_2H_2^+$ acetylene ions and C_2D_4 ethylene molecules. The amount of scrambled $C_2H_2D_2^+$ and $C_2HD_3^+$ products is much smaller and their relative intensity versus the non-scrambled $C_2D_4^+$ ions decreases with collision energy. This collision energy dependence clearly indicates that $C_2D_4^+$ products on one side, $C_2H_2D_2^+$ and $C_2HD_3^+$ products on the other side, come from two different reaction mechanisms. In the case of $C_4H_5^+$ product ions, the measured branching ratio between the two isotopomers slightly differs from the combinatorial calculated ratio, but a rigorous approach would require to take into account the zero point energies before drawing any further conclusion from this simple measurement.

3.4. Product ion time-of-flight spectra

Direct insight in the elementary reaction mechanism is obtained from the angular distribution of product ions. This is the reason why we measured the time-of-flight spectra for each product ion at several collision energies for the $C_2H_2^+ + C_2D_4$ reaction. Measured ion time-of-flight spectra are converted into velocity projection distributions along the detection axis and the results are shown in Figs. 5 and 6. In Fig. 5, results for

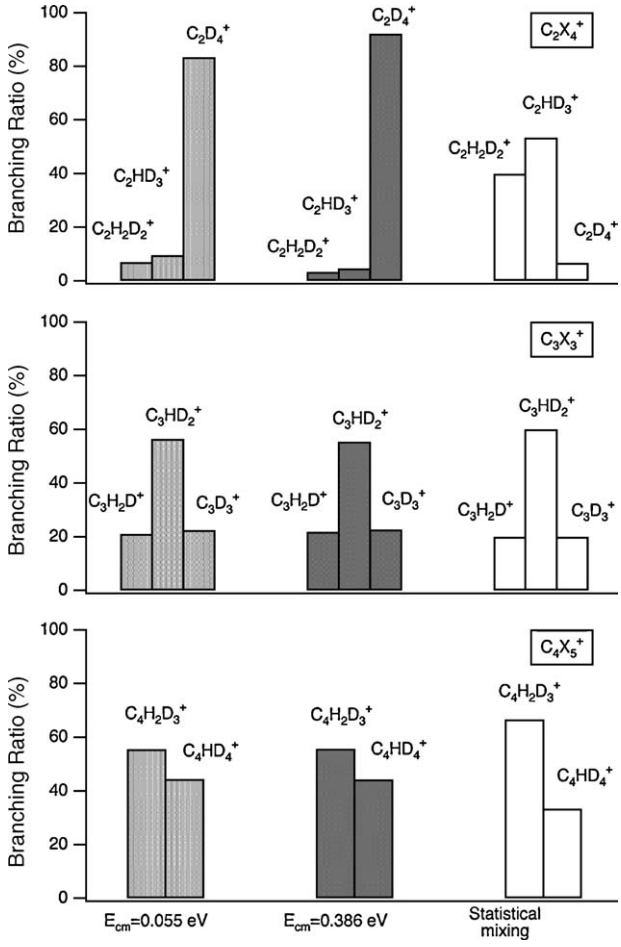

Fig. 4. Experimental branching ratio for the production of $C_2X_4^+$ (top), $C_3X_3^+$ (middle), and $C_4X_5^+$ (bottom) products where X = H or D in the $C_2H_2^+(X, v = 0) + C_2D_4$ reaction at two mean collision energies of 0.055 and 0.389 eV and calculated values using simple statistical assumptions (see text for details).

one isotopomer ion is plotted for each product ion: results for $C_2D_4^+$ product ions, which are the major ions for this reaction channel, $C_3HD_2^+$ in the case of the $C_3X_3^+$ formation and the sum of $C_4H_2D_3^+$ and $C_4H_2D_4^+$ in the case of the $C_4X_5^+$ product channel, in order to get better statistics. The centre of mass velocity projection is indicated as a dashed line and dot-dashed lines give nominal positions for backward and forward scattering along the detection axis, assuming the translational exoergicity to be equal to zero. All results for $C_3X_3^+$ and $C_4X_5^+$ product ions give velocity projection distributions, which are symmetric versus the centre of mass velocity at all collision energies. This is the signature of an elementary mechanism involving a long-lived intermediate complex. On the contrary, the velocity projection distribution for $C_2D_4^+$ product ions is asymmetric with a minor symmetric contribution, indicating an angular distribution, which is strongly backwards peaked. Such an angular distribution is expected for charge transfer occurring at long distance. The results for the three different $C_2X_4^+$ isotopomer ions are plotted in Fig. 6. The main $C_2D_4^+$ product ion exhibits asymmetric distributions, the two minor scrambled products giving symmetric distributions versus the centre of mass velocity. This clearly indicates that two different elementary reaction mech-

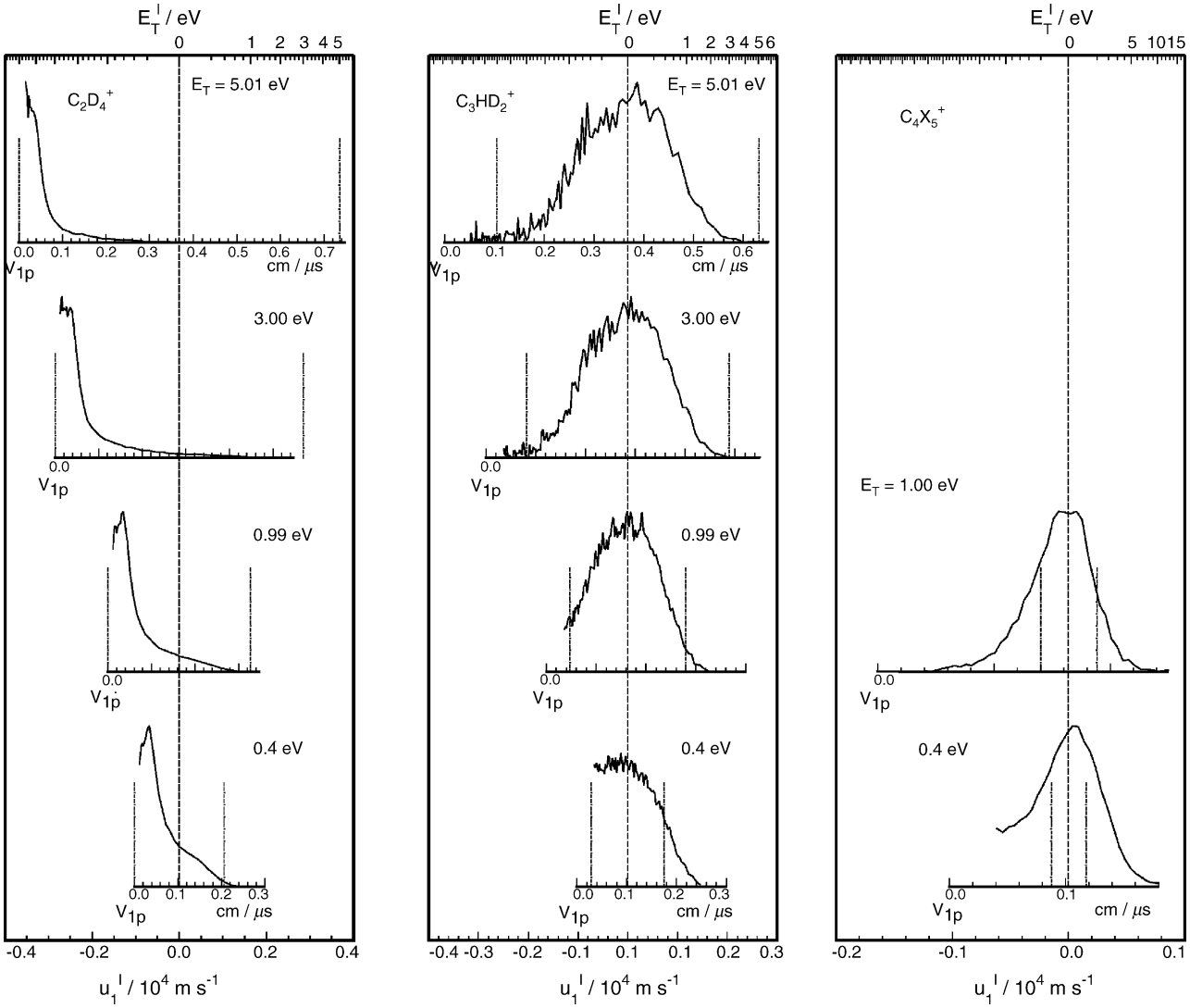

Fig. 5. Product velocity (u'_{1p}) or energy (E'_T) distributions in the centre of mass frame for $C_2D_4^+$ (left), $C_3HD_2^+$ (middle), and $C_4X_5^+$ (right) products where X = H or D in the $C_2H_2^+(X, v = 0) + C_2D_4$ reaction at different mean collision energies E_T as indicated in the figure. On each panel, the vertical dashed line represents the origin of velocities in the centre of mass frame and the two vertical dot-dashed lines represent the product velocity limits when the reactant and product kinetic energies are equal.

anisms are involved for the $C_2H_4^+$ product channel: the major mechanism corresponds to a long distance charge transfer producing $C_2D_4^+$ with no hydrogen atom scrambling and a minor mechanism involves a long lived intermediate complex producing the scrambled products.

3.5. Unimolecular and bimolecular statistical calculations

Even though among the three exothermic channels of the $C_2H_2^+ + C_2H_4$ reaction, the $C_2H_4^+ + C_2H_2$ product channel is a priori due to a charge transfer process which should be controlled by dynamics, we decided to perform statistical calculations. The main reason is that this system has been up to now considered as a test case for reactions controlled by statistics and modelled by the "transition state switching model" [6]. Jarrold et al. [6] have fitted the product branching ratios for both the unimolecular and bimolecular systems. As there are now much more precise experimental data, in particular absolute reaction cross-sections as a function of internal and collision energy, there are more constraints for the modelling. With this new information, we have revisited the calculations of Jarrold et al. [6] by using the same transition state switching model with the schematic chemical reaction path shown in Fig. 7. Along the reaction path, there are two transition states (TS): a tight transition state (TTS) close to the deep butadiene ion well and a loose orbiting transition state (OTS) located at the centrifugal barrier close to the separate products. At each collision energy and angular momentum, the rate limiting step is the transition state of minimum flux. In this model, $C_3H_3^+$ and $C_4H_5^+$ product ions come from the dissociation of $C_4H_6^+$ 1,3-butadiene ion, which corresponds to the deep well, whereas $C_2H_4^+$ ions come mainly from the dissociation of a less bound $(C_2H_2–C_2H_4)^+$ polarisation complex ion. In the bimolecular reaction, the first step is the formation of the polarisation complex, which can either dissociate into

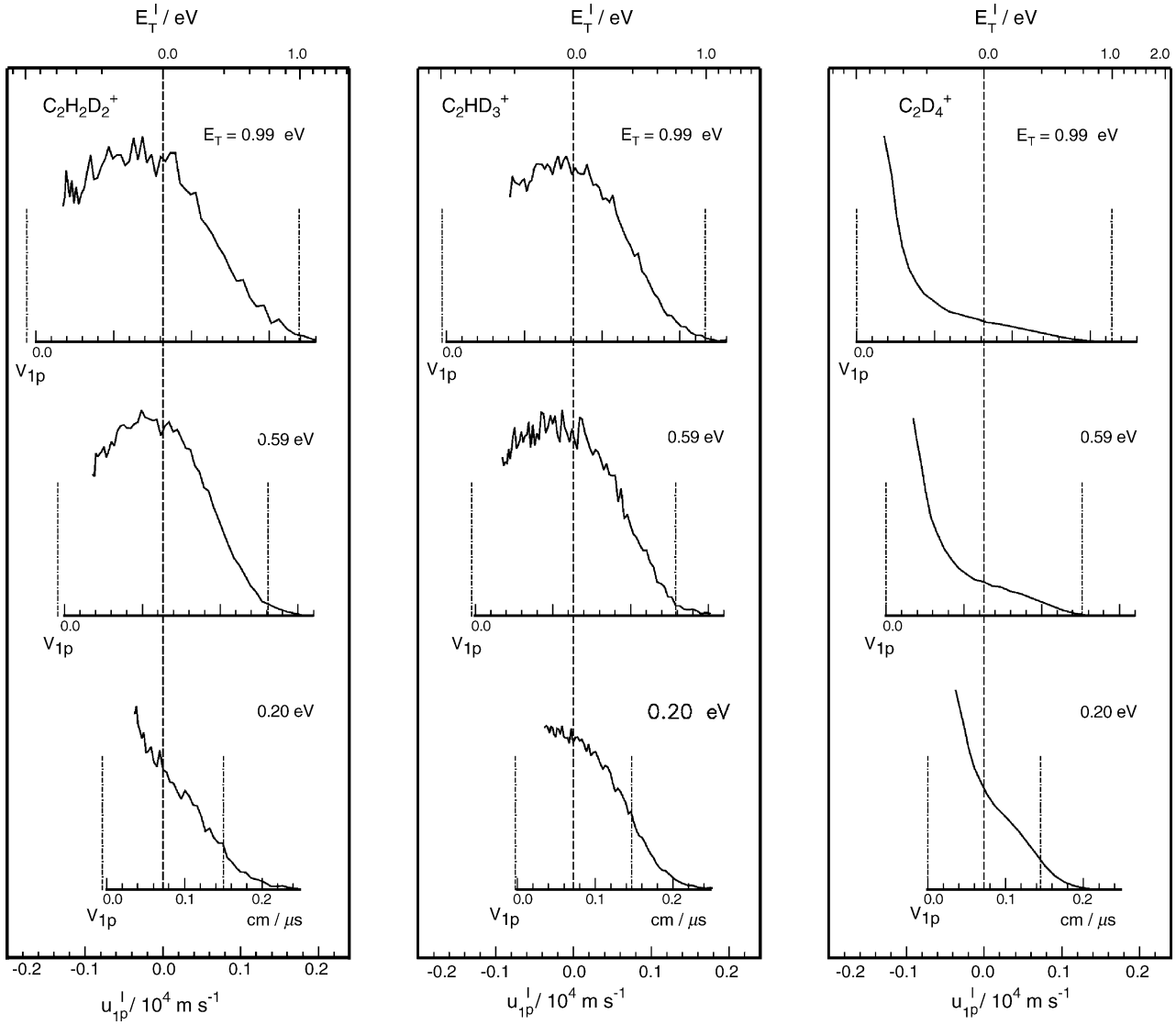

Fig. 6. Product velocity (u'_{1p}) or energy (E'_T) distributions in the centre of mass frame for $C_2H_2D_2^+$ (left), $C_2HD_3^+$ (middle), and $C_2D_4^+$ (right) products in the $C_2H_2^+(X, v = 0) + C_2D_4$ reaction at various mean collision energies E_T as indicated in the figure. Same indications as for Fig. 5 otherwise.

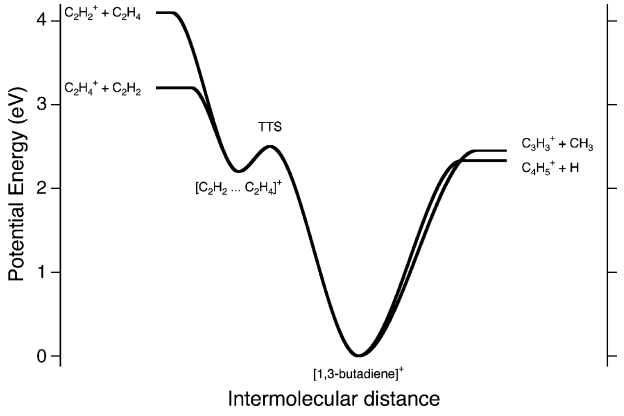

Fig. 7. Schematic cut of the potential energy surface for the $(C_4H_6)^+$ system connecting the main four product asymptotes along a reaction coordinate. A tight transition state (TTS) connects the deep 1,3-butadiene ion well and the polarisation complex $(C_2H_2 \cdots C_2H_4)^+$.

$C_2H_4^+ + C_2H_2$ or be followed by isomerization into butadiene ion prior to dissociation leading to $C_3H_3^+$ and $C_4H_5^+$ ions. These authors proposed this two-well model for two reasons. First, this is the only possibility for fitting the measured product branching ratios, which give $C_2H_4^+$ ions as the main products for the bimolecular reaction and as the minor ones for the unimolecular case. Secondly the only very partial H/D scrambling of the $C_2X_4^+$ products could be explained by assuming that there is complete scrambling in the deep well and no scrambling in the shallow well.

With this model, dissociation rates are calculated using the famous RRKM formula [1]:

$$k(E, J) = \sigma N^{\#}(E - E_J^{\#} - E_0)/h\rho(E - E_J)$$

where E is the total energy above the reactant, E_0 the transition state (TS) energy, E_J the rotational energy, which is

not available for the dissociation, $N^{\#}(E - E_J^{\#} - E_0)$ the number of internal states in the transition state between zero and $E - E_J^{\#} - E_0$, $\rho(E - E_J)$ the density of internal states in the reactant, h the Planck constant, and σ is the symmetry factor. This factor (ratio of reactant to TS symmetry numbers) compensates for the neglect of rotational symmetry in the calculation of densities and sums of states.

Dissociation rates are calculated using the QCPE 557 program package written by Chesnavich et al. [41]. This program uses the extended Beyer-Swinehard algorithm [42] to perform an exact quantum mechanical counting of the states. Vibrational degrees of freedom are treated as harmonic oscillators and rotations as rigid rotors. In the unimolecular calculations, C_4H_6 molecules are assumed to be in the vibrational ground state before ionization and a thermal distribution of the ions is assumed for the rotation. In the bimolecular calculations, no rotational energy is given to the C_2H_2 molecules before ionization and to the C_2H_4 target molecules before reaction. This is justified in this case, as we are in the limit where the total angular momentum is essentially equal to the orbital angular momentum. The thermal kinetic distribution is not included, because it is negligible compared to the mean collision energy. For both the unimolecular and bimolecular cases, integration over angular momentum is done using the Gauss–Legendre approximation. For a loose transition state, called orbiting transition state (OTS), the approximations of Klots [43] (low angular momentum limit) and of Grice et al. [44] (high angular momentum limit) are used, for the unimolecular case and bimolecular case, respectively.

We have profited from the relatively abundant information from the literature, to fix as many of the input parameters as possible. From kinetic energy release distributions, it is known that $C_4H_5^+$ has a reverse activation barrier of 0.25 eV, whereas $C_3H_3^+$ has none [6]. The $C_4H_5^+$ TS can be assumed to be a tight vibrator TS ($C_4H_5^+$–TTS) located at the top of the barrier. Most of the literature concerning the unimolecular reaction is focused on the dissociation path leading to CH_3 loss. Bowers and co-workers [6,45] used the transition state switching model to describe the change from a loose transition state (corresponding to the dissociation step) to a tight transition state (assigned by the authors to the isomerization from the 1,3-butadiene ion to the 3-methylcylopropene ion), as the internal energy of the $C_4H_6^+$ ion increases. This model implies that at higher internal energies, an isomerization reaction from the 1,3-butadiene ion leading to the 3-methylcylopropene ion should be rate limiting. While first efforts failed to confirm predictions based on this model [46], Russell et al. [47] found evidence for it and the more recent study of Keister et al. [27] concludes after comparison of the data to ab initio calculations that the tight transition state corresponds to a 1,4-hydrogen transfer from *cis*-1,3-butadiene to *cis*-1,3-diradical-butene. In addition, they also found a dissociation TS connecting the 3-methylcyclopropene ion with the associated complex c-$C_3H_3^+$–$^{\bullet}CH_3$. This loose TS is only of importance up to about 0.6 eV from the dissociation threshold. At much higher energies in the bimolecular reaction, the tight isomerization TS will therefore be entirely rate determining. The shallow polarisation well is connected to two product channels: $C_2H_2^+ + C_2H_4$ and $C_2H_4^+ + C_2H_2$. Both channels are treated as orbiting transition states (OTS) with the phase space theory (PST), the centrifugal barrier being dominant. The adjustable parameters are the energy and the frequencies of the TTS between the two wells. As the TTS structure is not known, its frequencies are obtained by multiplying the frequencies of the butadiene ion by a common factor. The main constraints for the parameters values are to fit both unimolecular and bimolecular ion product branching ratios, i.e., four kinds of experimental data: the butadiene ion breakdown diagram, the ion product branching ratios as a function of collision and internal energy, and the $C_2H_4^+$ product ratio coming from the deep well and from the shallow well. All those experimental data could be reasonably fitted with a common set of parameters. All input parameters and values of adjusted parameters, in particular the frequency multiplication factor, are given in Appendix A.

The calculated ion branching ratio for the butadiene ion fragmentation is shown in Fig. 3 (solid lines). If the $C_4H_6^+$, $C_4H_5^+$ and $C_3H_3^+$ are well fitted, it is not so good for $C_2H_4^+$. Our experimental measurement for this fragment ion abundance is well reproduced, but the steep rise from threshold measured by Bombach et al. [23] is very different from the smooth increase obtained in the calculations. It was not possible to perfectly fit the whole curve for this ion.

With the method of Chesnavich et al. [41], absolute reaction cross-sections are calculated by multiplying the product branching ratios by the Langevin capture cross-section. Therefore the total reaction cross-section as a function of collision energy is simply the calculated Langevin cross-section and cannot be compared to the experimental absolute cross-section values. As the Langevin capture model does not take into account the internal energy of the reactants, the calculated total reaction cross-section is a constant as a function of internal energy. Therefore calculations are compared to experimental ion product branching ratios and not to absolute cross-sections. Figs. 8 and 9 show the calculated branching ratios between the three ion products, as a function of collision energy and $C_2H_2^+$ internal energy, respectively. Calculations are shown as solid lines and experimental data as symbols. All those results are reasonably well fitted. It is not as good for the $C_2H_4^+$ ratio coming from the two wells, which is shown in Fig. 10 for collision energies up to 5 eV. The experimental data are derived from the D/H scrambling experiments with the assumption that there is complete statistical scrambling in the deep well and no scrambling in the shallow well. In this model, the small deviation between theory and experiment at low collision energies could be due to the existence of some scrambling in the shallow well.

Starting from $C_2H_4^+ + C_2H_2$, several isomerization steps are necessary to end up with the *trans*-1,3-butadiene ion structure, as shown by the intermediates and transition states ab initio calculations of Hrouda et al. [13]. So the present model with only two wells and one transition state is too simple. The activation energy resulting from the fit should therefore be considered as the TS corresponding to the rate limiting step. Among the calculated transition states, several structures could correspond to the 2.5 eV fitted activation energy, namely the TS 9 and TS 15 both connected to the trans-butadiene ion structure [13]. Both transition states involve a C–C bond forming between ethylene and

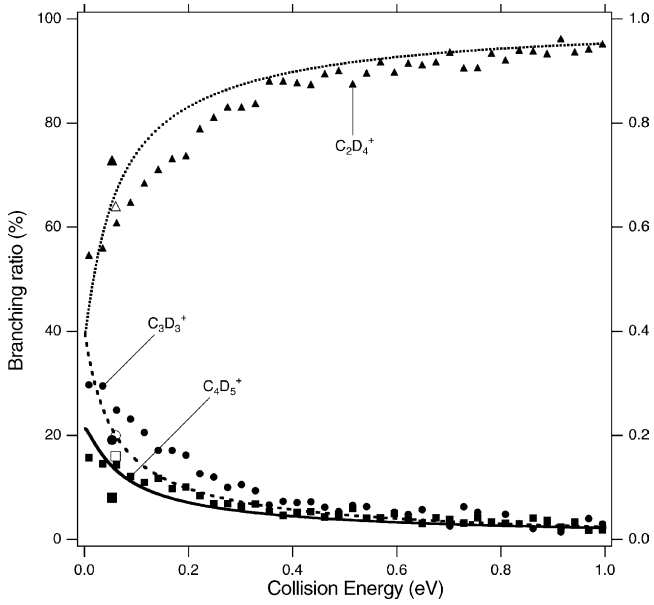

Fig. 8. Branching ratio as a function of collision energy for the production of $C_2D_4^+$ (triangles and dotted line), $C_3D_3^+$ (circles and dashed line), $C_4D_5^+$ (squares and full line) in the $C_2D_2^+(X, v = 0) + C_2D_4$ reaction: experimental values from [6] (open symbols) and from this work (full symbols: big symbols for coincidence experiments and small symbols otherwise) and RRKM calculations (lines) (see text for details).

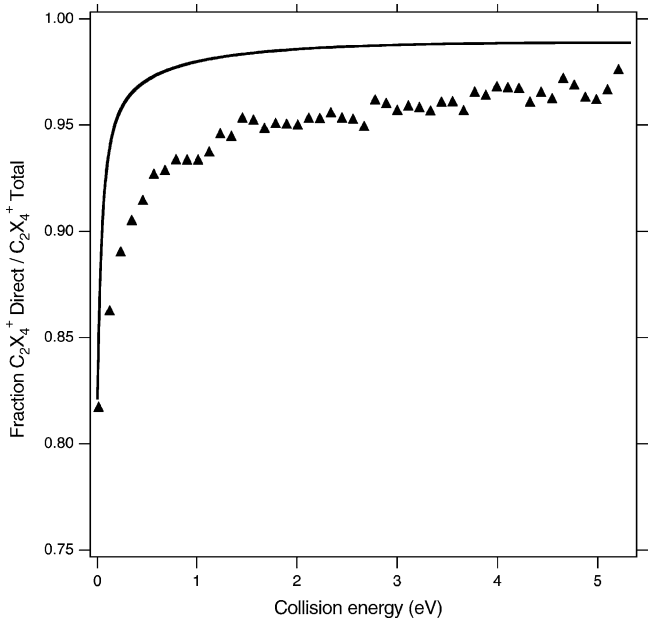

Fig. 10. Calculated fraction in the RRKM model (see text for details) of $C_2X_4^+$ products (full line) which have never experienced the deep well 1,3-butadiene ion compared to the experimental fraction of $C_2D_4^+$ products to all $C_2X_4^+$ products (X = H or D) from this work (triangles) in the $C_2H_2^+(X, v = 0) + C_2D_4$ reaction as a function of collision energy.

acetylene with an activation energy of about 2.6 eV, very close to the fitted value. Let us note that the fit does not correspond to a unique solution for the set of parameters, in particular the transition state frequencies. Therefore their values will not been discussed further.

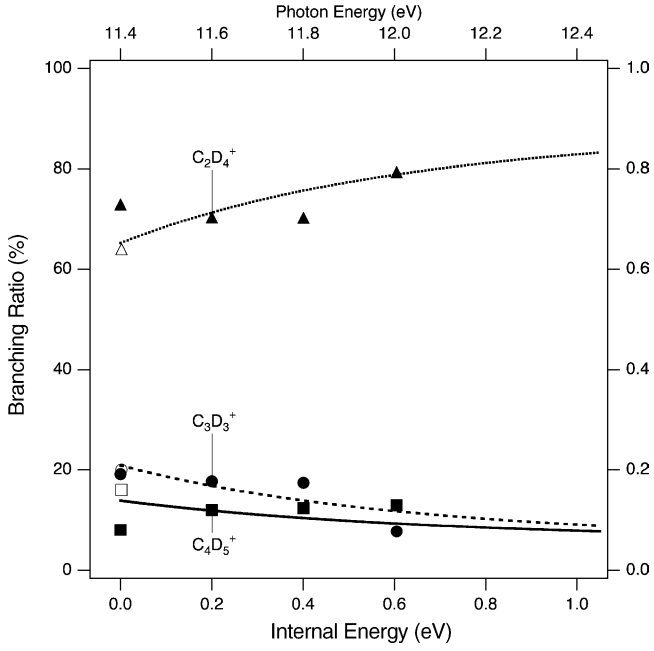

Fig. 9. Branching ratio as a function of $C_2D_2^+$ internal energy for the production of $C_2D_4^+$ (triangles and dotted line), $C_3D_3^+$ (circles and dashed line), $C_4D_5^+$ (squares and full line) in the $C_2D_2^+(X, v = 0) + C_2D_4$ reaction: experimental values from [6] (open symbols) and from this work (full symbols) and RRKM calculations (lines) (see text for details).

4. Discussion

Trying to simultaneously reproduce both uni- and bimolecular data with a single set of parameters in statistical calculations is a severe test for the validity of the model. The main challenge was to reproduce the fact that the major product ions in the bimolecular case are $C_2H_4^+$ ions, whereas they are the minor ones in the unimolecular case. Even though bimolecular collisions give access to a very different and much more variable range of total angular momenta as compared to unimolecular dissociations, the data could only be fitted by a double well model. However, the use of a statistical model is highly questionable because several experimental facts show that the intermediate complex leading to $C_2H_4^+$ products has a very short lifetime, which could not allow energy randomisation prior to dissociation. First the angular distribution of $C_2H_4^+$ ions are measured to be strongly backwards peaked versus the reactant ions, as observed for higher collision energies by Herman and Birkinshaw [18] in crossed beam studies. Secondly almost no scrambling is observed for the $C_2X_4^+$ products in D-atom labelled experiments. Moreover, statistical calculations cannot explain the increase as a function of internal energy of the reaction cross-sections for all three products. Finally the steep increase for the $C_2H_4^+$ ion in the butadiene ion breakdown curve cannot be reproduced by the calculations. Bombach et al. [23] already pointed out this problem and concluded that this fragment ion is not in competition with the other dissociation channels leading to $C_3H_3^+$ and $C_4H_5^+$ fragment ions. We completely agree with this and we think that a much more likely hypothesis is that $C_2H_4^+$ fragment ions come from a direct dissociation of an excited electronic state, which could be either the C ^2B_u state

which gives a strong band in the photoelectron spectrum in the 12.5–14.0 eV energy region [21]. So it is clear that only fitting product branching ratios for uni- and bimolecular reactions is not sufficient to conclude about the validity of the statistical model.

As a consequence, we propose an alternative model combining reaction control by both dynamics and statistics: (i) $C_2H_4^+$ ion products coming from a charge transfer process controlled by dynamics and (ii) $C_3H_3^+$ and $C_4H_5^+$ ion products coming from the dissociation of a long-lived intermediate complex well described by statistical models. We will now describe this model in more detail.

The observed backward–forward symmetry with respect to the centre of mass observed for the $C_3H_3^+$ and $C_4H_5^+$ product ions, as well as the complete scrambling of $C_3X_3^+$ and $C_4X_5^+$ isotopomers in D-labelled experiments, leaves little doubt that these products originate from a long-lived complex. Their relative abundance is also in good agreement with the one measured for the 1,3-butadiene ion dissociation. So those two products can be supposed to come from a long-lived intermediate complex which results from the isomerization into the most stable $C_4H_6^+$ structure, i.e., the 1,3-butadiene ion, and which can therefore be treated by a statistical model. However, there are several arguments in favour of a reaction control by dynamics for $C_2H_4^+$ product ions. The first and main argument comes from the strongly asymmetric angular distribution, which is the signature of a very short lifetime intermediate, shorter than the complex rotational period ($\tau = 10^{-12}$ to 10^{-13} s). It is thus very unlikely that intramolecular vibrational redistribution (IVR) leading to statistical redistribution of the energy prior to dissociation could take place in such a short time, in particular in a polarisation complex where low frequency intermolecular modes are badly coupled with high frequency molecular modes. Secondly, it is somewhat contradictory to invoke the absence of H atom scrambling in a loose polarisation complex and an implicit good coupling between loose and strong vibrational modes, which is required to legitimate the use of statistical theories. Thirdly, a statistical model implicitly supposes that there is no dynamical effect in the passage from the excited $C_2H_2^+ + C_2H_4$ potential energy surface to the ground potential energy surface leading to the $C_2H_4^+ + C_2H_2$ products, which is far to be obvious. Last but not least, statistical models cannot explain the increase of the absolute reaction cross-sections with internal energy of the reactant ions, as the calculated cross-sections follow the capture Langevin cross-section which varies only with collision energy. As this increase is measured for all three product ions, there must be a common step for all reaction channels, which could be the charge transfer.

Let us now investigate the possibility for an efficient charge transfer at large intermolecular distances, in order to explain the big charge transfer cross-sections. For this, two factors are required: near energy resonance between the entrance and exit reaction channels and, in first approximation, a good overlap between the vibrational wavefunctions of the reactants and products. It is not the case here as ionization potentials of acetylene and ethylene differ by 0.9 eV. In the equilibrium geometry of $C_2H_2^+$ and C_2H_4 at infinite separation of the reactants, the energy difference between the entrance and exit channels is calculated to be equal to 0.55 eV.[1] Therefore the entrance reaction channel unambiguously corresponds to the first excited potential energy surface of the system. This energy difference is still much too high to allow an electron jump at very large intermolecular distances. As the first excited electronic state of $C_2H_4^+$ is 1.87 eV above the ground state [48], it cannot play a role here. So the charge transfer must occur at shorter distance close to the potential energy surface crossing between the entrance and exit channels. If only the charge induced dipole interaction is taken into account and as the acetylene and ethylene polarisabilities are very close, there is no crossing between the excited state $C_2H_2^+ + C_2H_4$ and the ground state $C_2H_2 + C_2H_4^+$ potential energy curves at intermolecular distances where the reactants can be considered as separate entities (see Fig. 11). The crossing point is calculated at a distance of 1.6 Å, which is much smaller than any possible internuclear distance in a polarisation complex. However, with molecules such as acetylene and ethylene, one should add to the interaction potential a component due to the charge–quadrupole interaction. The most favourable orientation for this charge–quadrupole interaction is when an H atom of $C_2H_2^+$ points towards the C_2H_4 Π orbital, the $C_2H_2^+$ molecule axis being perpendicular to the ethylene molecular plane, as shown in Fig. 12a. If the ion–quadrupole interaction, which varies as 1/R3, is added to the $1/R^3$ ion-induced dipole interaction, the potential curve crossing is then calculated to

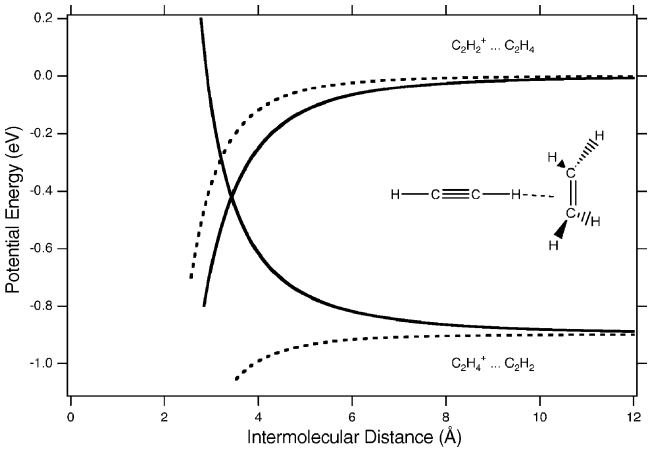

Fig. 11. Potential energy curves of the $(C_2H_2 \cdots C_2H_4)^+$ long range interaction: ion induced dipole interaction (dashed line) and with addition of the ion–quadrupole interaction, where acetylene is pointing toward the C–C ethylenic bond (full line). The energy origin is the $C_2H_2^+ + C_2H_4$ asymptote.

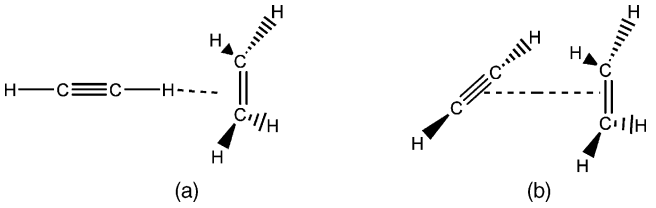

Fig. 12. Two C_2H_2 and C_2H_4 relative geometries with the acetylene either pointing toward the C–C ethylenic bond (a) or parallel to the ethylene plan (b).

[1] P. Maître, 2005, Personal communication.

Table 2
Calculated R_{max} values for the intermolecular distances between the molecule centres of mass as a function of collision energy for two types of interaction potentials

E_{cm} (eV)	R_{max} [a] (Å)	R_{max} [b] (Å)
0.1	4.17	4.63
0.2	3.51	3.84
0.3	3.17	3.40
0.4	2.95	3.13
0.5	2.79	2.94
0.6	2.67	2.79
0.7	2.57	2.67
0.8	2.48	2.58
1.0	2.34	2.42

[a] R_{max} calculated with the ion-induced dipole interaction.
[b] R_{max} calculated with the ion-induced dipole plus the ion–quadrupole interaction.

be at 3.45 Å (see Fig. 11), instead of the previously calculated 1.6 Å value (see Appendix B). A possible electron jump at such an interaction distance could now well explain the measured charge transfer cross-sections. Let us note that, as the calculation is made for the maximum ion–quadrupole interaction, any other reactant orientation would give a crossing point at shorter intermolecular distance.

The next question is whether the charge transfer occurs before or after the capture in the reactants approach. The capture distance can be calculated with the Langevin model, which was originally proposed for atom–atom reactions [8]. With this model, for ion–molecule reactions that have no barrier, the R_{max} distance for which there is capture is calculated as a function of collision energy, by taking into account the attractive interaction potential and the centrifugal barrier. Very often this calculation is done with only the ion-induced dipole interaction potential. As shown above, it is necessary to also include the ion–quadrupole interaction. Table 2 gives the calculated R_{max} values as a function of the collision energy E_{cm} for both types of interaction potentials. In the case of the more realistic potential taking into account the ion–quadrupole interaction, the calculated distance for capture is bigger than the potential curve crossing one, for collision energies up to around 0.3 eV. It is thus reasonable to suppose that the first step in the approach is the capture, which is followed by charge transfer. As the calculated distance for charge transfer is a maximum value, capture most probably precedes the electron jump at collision energies up to about 1 eV. Note that the favourable orientation for charge transfer from $C_2H_2^+$ to C_2H_4 (Fig. 12a) becomes repulsive for the $C_2H_4^+$–C_2H_2 system, for which one of the most stable loosely bound complex has a T shape structure [13] as shown in Fig. 12b. Therefore, as soon as there is electron jump, the system tends to separate the reactants. A mechanism involving capture prior to the charge transfer is probably rather general for non-resonant charge transfer reactions, even in the case of small systems, when the electron jump is not possible at large internuclear distances. Let us now compare the calculated capture cross-section with the measured total reaction cross-section (see Fig. 13). The experimental total reaction cross-section variation with collision energy is very similar to the one of the Langevin cross-section and not very different for both types of interaction potentials. If we compare the total absolute reaction cross-sections to the Langevin capture cross-section calculated with an ion-induced dipole interaction, one would have concluded that this reaction was very efficient ($\sigma_{total}/\sigma_{capture}$ about equal to 0.7). With the ion–quadrupole interaction, this ratio becomes equal to 0.5, which is a minimum value, as the calculated capture cross-section is a maximum value in this case. So the reaction efficiency is high anyway. Let us note that, if charge transfer was taking place before the capture in the reactant approach, the total cross-section would have no reason to follow the Langevin cross-section variation trend with collision energy. As the $\sigma_{total}/\sigma_{capture}$ ratio is constant within experimental errors, it is reasonable to suppose that capture always precedes charge transfer in the whole collision energy range investigated in the present study.

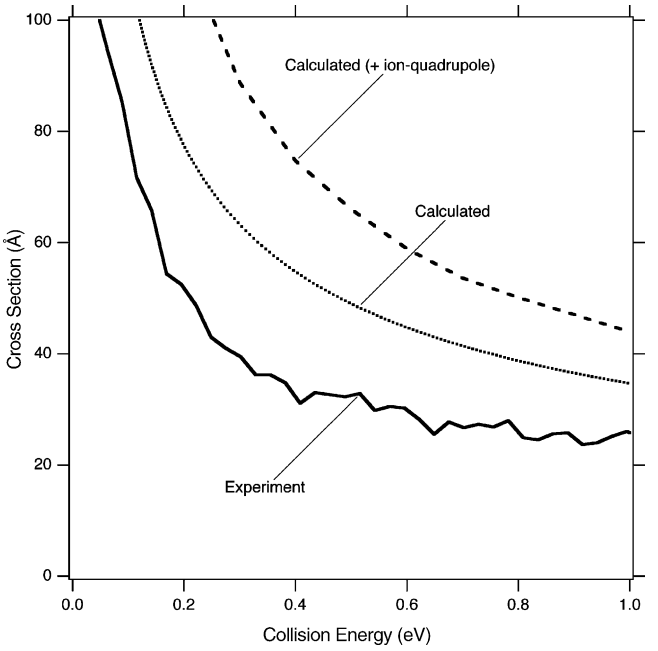

Fig. 13. Total cross-sections as a function of collision energy for the $C_2D_2^+(X, v = 0) + C_2D_4$ reaction: experimental results (full line) compared to the calculated capture cross-section, using the ion induced dipole interaction only (dotted line) or with the addition of the ion–quadrupole interaction (dashed line).

In the reactant approach, the proposed reaction path consists of the following sequences. The first step is the capture between the reactants, which is followed by charge transfer. Then, according to the relative orientation of the two molecules, either there is fast separation between the reactants giving $C_2H_4^+$ and C_2H_2 products, or there are several steps of isomerization leading to the 1,3-butadiene ion structure which dissociates into $C_4H_5^+ + H$ and $C_3H_3^+ + CH_3$. This is illustrated by the reaction path model shown in Fig. 14. In previous papers concerning this reaction, charge transfer has been supposed to precede the isomerization into butadiene ion [13]. In the potential energy surface region leading to the 1,3-butadiene ion structure, there are most probably several isomerization steps [13], which are schematically represented in a circle in Fig. 14 by only one shallow well and one transition state towards the deep well. This alterna-

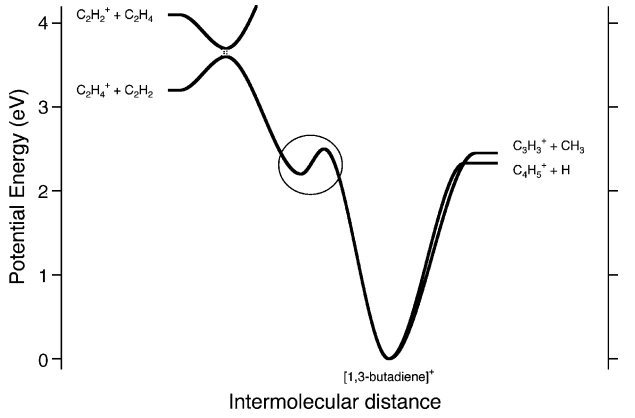

Fig. 14. New schematic cut of the potential energy surface for the $(C_4H_6)^+$ system including the $(C_2H_2\cdots C_2H_4)^+$ charge transfer interaction curves. The well and transition state inside the circle represent schematically several wells and transition states between the entrance channel and the deep 1,3-butadiene ion well.

tive model is consistent with all experimental observations: (i) the same variation trend of reaction cross-sections versus collision or internal energy for the three products; (ii) the product ion angular distributions (peaked for $C_2H_4^+$ and isotropic for $C_3H_3^+$ and $C_4H_5^+$); (iii) the H/D scrambling results. Let us note that there is a very small amount of $C_2X_4^+$ products for which there is H/D scrambling and which have an isotropic angular distribution. These products come from some trajectories which explore the deep butadiene ion well, before coming back and exit into $C_2X_4^+ + C_2X_2$ products. Last the increase of the reaction cross-section with internal energy is probably a dynamical effect in the charge transfer process, which would require further dynamics theoretical calculations with more complete ab initio potential energy surfaces. In our model, as charge transfer precedes the isomerization towards the butadiene ion structure leading to the $C_3H_3^+$ and $C_4H_5^+$ products, their relative cross-sections follow the charge transfer variation with reactant internal energy.

5. Conclusion

In conclusion, the present study showed that the $C_2H_2^+ + C_2H_4$ reaction which was up to now considered as controlled by statistics, is in fact controlled by both dynamics and statistics. Dynamical effects are mainly due to the fact that the entrance reaction channel corresponds to an excited potential energy surface. We propose an alternative model for its elementary mechanism involving first a dynamical step in the reactant approach followed by several possible reaction routes, one of them leading to a deep potential well, where statistical models can be applied. This reaction is a good example to show that a good fit of reaction branching ratios by statistical theories is not sufficient to conclude about the reaction mechanism. In order to test possible dynamical effects, it is mandatory to have precise experimental data, in particular product angular distributions, internal energy effects on the reactivity such as for instance vibrational mode specificity and product internal energy states. Reaction mechanisms combining control by both dynamics and statistics are most probably more frequent than expected for polyatomic reactants. In particular, dynamical effects are very probable for reactions starting on an excited potential energy surface, as for the $C_2H_2^+ + C_2H_4$ reaction. Moreover, polarisation complexes, which have been developed for atom–atom or atom–diatom systems, are too simple for polyatomic systems. In this case, the relative orientation of reactants can play an essential role, as shown with our simple model involving the ion–quadrupole interaction. This is well known in organic chemistry, but should now be more often considered in dynamical studies.

Acknowledgements

We would like to thank D. Gerlich and S. Mark for the time-of-flight spectra which were recorded by HP in his laboratory. This work is a long story with many very helpful discussions over the years with colleagues, who are deeply thanked: Y.T. Lee, C.E. Klots, T. Baer, W.L. Hase, S.L. Anderson, Z. Herman; H.-E. Audier, J.M. Mestdagh, P. Parneix. This paper would not have existed without them. R. Thissen is also thanked for his help in reading the manuscript. The LURE staff is acknowledged for running the Super-ACO storage ring and general facilities.

Appendix A. Parameters for unimolecular and bimolecular statistical calculations

E_0 is the transition state energy, σ the symmetry factor, B the rotational constant, and σ is the polarisability.

- Species 1: $C_4H_6^+$ *trans*-1,3-butadiene ion ($E_0 = 0$ eV, $\sigma = 2$, $B = 0.304\ \text{cm}^{-1}$)
  Vibrational frequencies (cm^{-1}) [49]

3101	3087	3055	3003	2992
2884	1630	1596	1438	1381
1294	1280	1196	1013	990
976	912	908	894	770
522	512	301	162	

- Species 2: OTS $C_3H_3^+ + CH_3$ loose transition state ($E_0 = 2.40$ eV, $\sigma = 36$, $B(CH_3) = 7.61\ \text{cm}^{-1}$, $B(C_3H_3) = 0.8\ \text{cm}^{-1}$, $\alpha(CH_3) = 2.2\ \text{Å}^3$)
  Vibrational frequencies (cm^{-1}) [6]

3160	3160	3050	3050	3050
3040	1550	1400	1400	1200
1200	1150	1150	1000	1000
800	800	620		

- Species 3: TTS $C_3H_3^+ + CH_3$ tight transition state; 1-methylcyclopropene ion structure ($E_0 = 2.19$ eV, $\sigma = 1$, $B = 0.33\ \text{cm}^{-1}$)
  Vibrational frequencies (cm^{-1}) [50]

3133	3071	3049	2973	2929
2895	1788	1487	1450	1400
1032	964	950	919	696
331	283	170		

- Species 4: TTS $C_4H_5^+ + H$ tight transition state; 1-methylcyclopropene ion structure ($E_0 = 2.30$ eV, $\sigma = 1$, $B = 0.27\ cm^{-1}$)
  Vibrational frequencies (cm^{-1}) [50]

3133	3071	3049	2973	2929
2895	1788	1487	1450	1400
1032	964	950	919	696
331	283	170		

Multiplication factor: 1.3 for the three last frequencies.

- Species 5: OTS $C_2H_4^+ + C_2H_2$ orbiting transition state ($E_0 = 3.20$ eV, $\sigma = 8$, $B(C_2H_4) = 1.78\ cm^{-1}$, $B(C_2H_2) = 1.18\ cm^{-1}$, $\alpha(C_2H_2) = 3.33\ Å^3$)
  Vibrational frequencies (cm^{-1}) [6]

3370	3290	3100	3100	3000
3000	1970	1450	1450	1230
1230	950	950	810	730
730	610	610	300	

Multiplication factor: 1.17 for all frequencies.

- Species 6: OTS $C_2H_2^+ + C_2H_4$ orbiting transition state ($E_0 = 4.10$ eV, $\sigma = 8$, $B(C_2H_4) = 1.78\ cm^{-1}$, $B(C_2H_2) = 1.18\ cm^{-1}$, $\alpha(C_2H_4) = 4.22\ Å^3$)
  Vibrational frequencies (cm^{-1}) [6]

3370	3290	3100	3011	3000
3000	1830	1620	1440	1340
1240	1030	950	950	810
800	800	650	650	

- Species 7: TTS $(C_2H_2 + C_2H_4)^+$ tight transition state ($E_0 = 2.50$ eV, $\sigma = 1$, $B = 0.30\ cm^{-1}$)
  Vibrational frequencies (cm^{-1}) [6]

3310	3230	3060	3060	2980
2980	1870	1450	1450	1200
1200	960	920	870	870
770	670	670	380	300
275	225	75		

Multiplication factor: 1.2 for all frequencies.

Appendix B. Representation of the quadrupolar tensor of acetylene and ethylene by a charge ensemble

B.1. Acetylene

Its quadrupolar tensor has only one independent component, along the z molecular axis:

$$\Theta_{zz} = 2q(r_2^2 - r_1^2)$$

where q is the charge, $r_1 = r_{CC}/2$ with r_{CC} being the C–C distance, and $r_2 = r_{CC}/2 + r_{CH}$, r_{CH} being the C–H distance. With $+q$ ($q > 0$) charge on H atoms and $-q$ charge on carbon atoms and using the experimental value for the quadrupolar tensor [51], one obtains $q = 0.273$ a.u.

B.2. Ethylene

Its quadrupolar tensor has two independent components along the z molecular axis and the x axis perpendicular to the C–C bond:

$$\Theta_{xx} = q(r_1^2 + 2r_2^2 - r_3^2), \qquad \Theta_{zz} = q(2r_3^2 - r_2^2 - 2r_1^2)$$

where $r_1 = r_{CC}/2$, $r_2 = \sin\theta\, r_{CH}$ and $r_3 = r_{CC}/2 + \cos\theta\, r_{CH}$, with θ being the angle between the CH and the CC bonds.

We chose to put $-q'$ ($q' > 0$) on each carbon atom and $q'' = q'/2$ in the plane of the molecule at a distance from each carbon atom equal to the CH bond length. The θ angle is the other unknown of the problem. Using the experimental values of the quadrupolar tensor [52], one obtains $q'' = 0.1785$ a.u. and $2\theta = 124°$.

Let us note that the H atoms in acetylene carry more positive charge than those of ethylene, which is expected from a chemical intuition point of view. Moreover the 2θ angle is very close to the HCH angle value of 117° in ethylene [53].

References

[1] T. Baer, W.L. Hase, Unimolecular Reaction Dynamics, Oxford University Press, New York, 1996.
[2] W.L. Hase, Acc. Chem. Res. 31 (1998) 659.
[3] H.W. Schranz, T.D. Sewell, J. Mol. Struct. (Theochem.) 368 (1996) 125.
[4] L. Sun, K. Song, W.L. Hase, Science 296 (2002) 875.
[5] J. Liu, S.L. Anderson, Int. J. Mass Spectrom. 241 (2005) 173.
[6] M.F. Jarrold, L.M. Brass, P.R. Kemper, P.A.M. van Koppen, M.T. Bowers, J. Chem. Phys. 78 (1983) 3756.
[7] H. Palm, Thesis, Université Paris-Sud, Orsay, 1996.
[8] R.D. Levine, R.B. Bernstein, Molecular Reaction Dynamics and Chemical Reactivity, Oxford University Press, New York, 1987.
[9] C. Lifshitz, Chem. Soc. Rev. 30 (2001) 186.
[10] Y. Hu, B. Hadas, M. Davidovitz, B. Balta, C. Lifshitz, J. Phys. Chem. A 107 (2003) 6507.
[11] C. Galloy, C. Lecomte, J.C. Lorquet, J. Chem. Phys. 77 (1982) 4522.
[12] W.J. Chesnavich, L. Bass, T. Su, M.T. Bowers, J. Chem. Phys. 74 (1981) 2228.
[13] V. Hrouda, P. Carsky, M. Ingr, Z. Chval, G.N. Sastry, T. Bally, J. Phys. Chem. A 102 (1998) 9297.
[14] J.C. Lorquet, Int. J. Mass Spectrom. 200 (2000) 43.
[15] O. Dutuit, M. Aït-Kaci, J. Lemaire, M. Richard-Viard, Phys. Scripta T31 (1990) 223.
[16] O. Dutuit, S.C. NATO ASI Series, Fundam. Gas Phase Ion Chem., Kluwer Academic Press, 1991, p. 21.
[17] S.L. Anderson, Acc. Chem. Res. 30 (1997) 28.
[18] Z. Herman, K. Birkinshaw, Ber. Buns. Phys. Chem. 77 (1973) 566.
[19] V.G. Kim, V.G. Anicich, W.T. Huntress, J. Chem. Phys. 81 (1977) 1978.
[20] A.S. Werner, T. Baer, J. Chem. Phys. 62 (1975) 2900.
[21] J. Dannacher, J.-P. Flamme, J.-P. Stadelmann, J. Vogt, Chem. Phys. 51 (1980) 189.
[22] F.N. Preuninger, J.M. Farrar, J. Chem. Phys. 77 (1982) 263.
[23] R. Bombach, J. Dannacher, J.-P. Stadelmann, J. Am. Chem. Soc. 105 (1983) 1824.
[24] A.M. Woodward, W.A. Chupka, S.D. Colson, J. Phys. Chem. A 88 (1984) 4567.
[25] T.L. Bunn, T. Baer, J. Chem. Phys. 85 (1986) 6361.
[26] T.L. Bunn, M.T. Bowers, J. Phys. Chem. A 92 (1988) 1813.
[27] J.W. Keister, T. Baer, M. Evans, C.Y. Ng, C.W. Hsu, J. Phys. Chem. A 101 (1997) 1866.
[28] S. Lias, J. Bartness, J. Liebmann, J. Holmes, R. Levin, W. Mallard, J. Phys. Chem. Ref. Data 17 (1988).

[29] O. Dutuit, C. Alcaraz, D. Gerlich, P.M. Guyon, J. Hepburn, C. Metayer-Zeitoun, J.B. Ozenne, M. Schweizer, T. Weng, Chem. Phys. 209 (1996) 177.
[30] M. Richard-Viard, O. Dutuit, M. Lavollée, T. Govers, P.M. Guyon, J. Durup, J. Chem. Phys. 82 (1985) 4054.
[31] E. Teloy, D. Gerlich, Chem. Phys. 4 (1974) 417.
[32] D. Gerlich, State-Selected and State-to-State Ion–Molecule Reaction Dynamics. Part 1. Experiment, John Wiley, New York, 1992, p. 1.
[33] G. Henri, M. Lavollée, O. Dutuit, J.B. Ozenne, P.M. Guyon, E.A. Gislason, J. Chem. Phys. 88 (1988) 6381.
[34] S. Mark, D. Gerlich, Chem. Phys. 209 (1996) 235.
[35] K.M. Ervin, P. Armentrout, J. Chem. Phys. 83 (1985) 166.
[36] C. Métayer-Zeitoun, C. Alcaraz, S.L. Anderson, H. Palm, O. Dutuit, J. Phys. Chem. A 99 (1995) 15523.
[37] C.Y. Ng, State-Selected and State-to-State Ion–Molecule Reaction Dynamics. Part 1. Experimental, John Wiley, New York, 1992, p. 401.
[38] I. Koyano, K. Tanaka, State-Selected and State-to-State Ion–Molecule Reaction Dynamics. Part 1. Experimental, John Wiley, New York, 1992, p. 263.
[39] P.M. Guyon, E.A. Gislason, Topics in Current Chemistry, Springer, Berlin, 1989, p. 161.
[40] M. Richard-Viard, A. Delboulbé, M. Vervloet, Chem. Phys. 209 (1996) 159.
[41] W.J. Chesnavich, L. Bass, G.M. E., K. Song, D.A. Webb, QCPE 557 TSTPST: Statistical theory package for RRKM/TST/PST calculations, Indiana University, 1988.
[42] S.E. Stein, B.S. Rabinovitch, J. Phys. Chem. A 58 (1973) 2438.
[43] C.E. Klots, Kinetics of Ion–Molecule Reactions, Plenum Press, New York, 1979.
[44] M.E. Grice, K. Song, W.J. Chesnavich, J. Phys. Chem. A 90 (1986) 3503.
[45] W.J. Chesnavich, M.T. Bowers, J. Am. Chem. Soc. 99 (1977) 1705.
[46] T. Baer, J. Electr. Spectrosc. Rel. Phenom. 15 (1979) 225.
[47] D.H. Russell, M.L. Gross, J. van der Greef, N.M.M. Nibbering, J. Am. Chem. Soc. 101 (1979) 2086.
[48] D.W. Turner, C. Baker, A.D. Baker, C.R. Brundle, Molecular Photoelectron Spectroscopy, John Wiley, New York, 1970.
[49] T. Shimanouchi, Tables of Molecular Vibrational Frequencies, L.M. Kushner, Washington, 1972.
[50] R.W. Mitchell, J.A. Merritt, Spectrochim. Acta 25A (1969) 1881.
[51] A. Halkier, S. Coriani, Chem. Phys. Lett. 303 (1999) 408.
[52] D.H. Russell, M.A. Spackman, Mol. Phys. 98 (2000) 855.
[53] C.W. Bauschlicher Jr., S.R. Langhoff, J. Phys. Chem. A 95 (1991) 2278.